Fixation of Buried and Surface-Mounted Magnets in High-Speed Permanent-Magnet Synchronous Machines

Andreas Binder, *Senior Member, IEEE*, Tobias Schneider, and Markus Klohr

***Abstract*—High-speed applications involve technical and economical advantages because, as direct drives, they avoid the gear as an additional mechanical drive component. Permanent-magnet synchronous machines (PMSMs) are attracting growing attention for high-speed drives. Surface-mounted PMSMs request a glass- or carbon-fiber bandage to fasten the magnets to the rotor surface at high speed. At rotors with "buried" magnets, the rotor iron itself fixes the magnets. This paper presents simple calculation strategies and discusses their limits for the mechanical design of high-speed machines with either surface-mounted or buried magnets. The results of the calculations are compared with finite-element calculations.**

***Index Terms*—High-speed machines, magnetic levitation, permanent-magnet machines.**

I. Introduction

USING compact high-speed motors instead of geared standard motors, e.g., compressors or vacuum pumps, reduces the number of drive components, increases system reliability, and offers the opportunity to reduce costs. The main benefits of gearless directly coupled high-speed machines are the prevention of gear costs, oil leakage, gear maintenance, and gear losses. Furthermore, noise can also be reduced significantly by avoiding an additional transmission system. As high-speed machines generate high power from high rotational speed but small torque, small and very compact motors allow for new integrated drive constructions. Examples for the application of directly coupled high-speed machines are as follows:

- high-speed cutting in tooling machines;
- compressors;
- high-speed generators in microgasturbines for the currently discussed decentralized power supply;
- motor–generators for flywheel applications;
- starter generators for aircraft engines;
- drives for balancing machines, etc.

Paper IPCSD-06-025, presented at the 2005 Industry Applications Society Annual Meeting, Hong Kong, October 2–6, and approved for publication in the IEEE TRANSACTIONS ON INDUSTRY APPLICATIONS by the Electric Machines Committee of the IEEE Industry Applications Society. Manuscript submitted for review October 15, 2005 and released for publication March 29, 2006.

A. Binder and T. Schneider are with the Institute of Electrical Energy Conversion, Darmstadt University of Technology, 64283 Darmstadt, Germany (e-mail: abinder@ew.tu-darmstadt.de; tschneider@ew.tu-darmstadt.de).

M. Klohr was with the Institute of Electrical Energy Conversion, Darmstadt University of Technology, 64283 Darmstadt, Germany. He is now with Bombardier Transportation, 68309 Mannheim, Germany (e-mail: markus.klohr@de.transport.bombardier.com).

Digital Object Identifier 10.1109/TIA.2006.876072

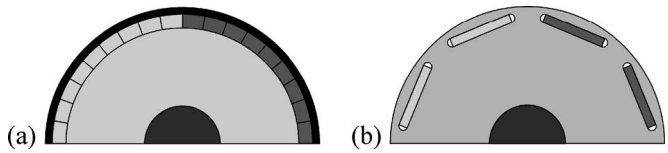

Fig. 1. (a) Surface-mounted magnet and (b) buried magnet synchronous rotors.

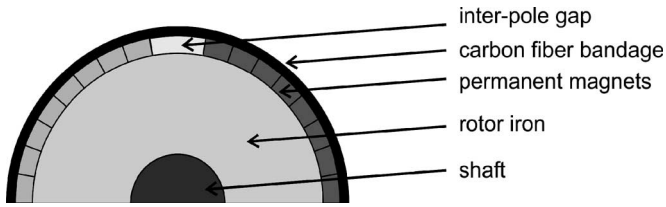

Fig. 2. Axial cross section of a PMSM with carbon-fiber bandage ($\alpha_e < 1$).

Different ac motor concepts are qualified for high-speed applications, such as squirrel cage induction motors, e.g., with massive rotors, permanent-magnet synchronous machines (PMSMs) or homopolar synchronous machines, and switched reluctance machines. Nowadays, PMSMs are becoming more and more favored. Due to the nonelectric excitation, rotor losses are very small, leading to minor thermal rotor expansion and to an increased efficiency. However, high-speed direct drives require special motor designs, especially with respect to mechanical issues, to be able to withstand high mechanical stress. In the case of a PMSM, two different rotor constructions, namely: 1) surface-mounted magnets and 2) buried magnets (Fig. 1), can be distinguished and need different design procedures.

II. Bandage Design for Surface-Mounted Magnet High-Speed Machines

Fig. 2 shows an axial cross section of a PMSM with permanent magnets glued onto the rotor surface and fixed by a carbon- or glass-fiber bandage. To achieve a defined prestress and therefore a defined contact force, bandages are designed as prefabricated sleeves made from either glass or carbon fiber, which is embedded within an epoxy resin matrix. At a circumferential speed typically above 150 m/s, the strength of glass-fiber bandages is not sufficient anymore to safely fix the magnets to the rotor surface. In these cases, the carbon-fiber technology with maximum permissible tension of the fibre-matrix composite of $\sigma_{t,\max} = 1100$ N/mm^2 (including deterioration effect due to manufacturing) is a high-quality

TABLE I
COMPARISON OF GLASS- AND CARBON-FIBER MATERIALS

Material	E_{11} [GPa]	E_{12} [GPa]	$\sigma_{t,max}$ [N/mm^2]
Glass fibre GF	73	73	2400 (20°C)
Carbon fibre CF	240	16.4	4800 (20°C)
60% CF matrix	142	9.7	2475 (20°C)
55% CF matrix	132	8.8	-
	temperature influence		1650 (150°C)
	manufacturing influence		1100 (150°C)

alternative [1] (Table I). With respect to the rotor outer diameter d_a, the sleeve has a small undersize ΔD. The assembly of the rotor is done by either axial pressing or cold shrinking of the sleeve onto the rotor. The contact force due to the glue is neglected in the following, as—due to the large number of magnets—it may vary from magnet to magnet, thus being uncertain. The mechanical stress of the bandage is mainly in the form of tangential tensile stress σ_t. If the rotor is designed with an interpole gap (pole coverage ratio $\alpha_e < 1$), additional bending load occurs at the magnet edges. In an overspeed test, the bandage has to withstand centrifugal forces at 20% overspeed for 2 min and must provide a positive residual contact pressure p_c between the magnets and the rotor iron. It must be assured that the maximum permissible tangential stress inside the bandage is not exceeded. These two fundamental conditions for the mechanical stability of a high-speed permanent-magnet rotor at overspeed are described by

$$p_c(n = n_{\text{overspeed}}) = p_{c,\text{prestress}} - p_{\omega,m} - p_{\omega,b} > 0 \quad (1)$$

$$\sigma_t(n = n_{\text{overspeed}}) = \sigma_{t,\text{prestress}} + \sigma_{t,\omega} < \sigma_{t,\max}. \quad (2)$$

For simple but realistic rotor configurations with rotational symmetry, the bandage design can be done using the following formulas [2]. For more detailed investigations in case of rotors with an interpole gap or with influence of magnet edges pressing against the bandage, more elaborate analytical or finite-element (FE) calculations are necessary. Using Young's modulus E, the sleeve undersize ΔD, and the bandage height h_b, the prestress and the contact pressure due to shrinking or pressing of the sleeve onto the rotor is given by (3) and (4a), if the bandage is considered as a "thin shell." If the bandage is considered as a "thick shell," (4b) needs to be employed [3], i.e.,

$$\sigma_{t,\text{prestress}} = \varepsilon \cdot E = \frac{\Delta D}{d_a} \cdot E \quad (3)$$

$$p_{c,\text{prestess}} = \frac{\sigma_{t,\text{prestress}} \cdot h_b}{r_b} \quad \text{(thin shell)} \quad (4a)$$

$$p_{c,\text{prestess}}(r) = \sigma_{t,\text{prestress}} \cdot \left(\frac{r_i^2}{r_a^2 - r_i^2} \cdot \left(1 + \frac{r_a^2}{r^2} \right) \right)^{-1} \quad \text{(thick shell)}. \quad (4b)$$

Here, h_b and r_b represent height and average radius of the bandage, whereas r_i and r_a are the inner and outer bandage radii, respectively. Whereas glass-fiber Young's modulus is nearly the same in radial E_{11} and tangential E_{12} directions ("isotropic shell," $E_{11} = E_{12}$), for carbon fiber, these values differ considerably ("orthotropic shell," $E_{11} \gg E_{12}$, Table I). Equations (3)–(5) do not consider this effect. Heating of the rotor components during operation by, e.g., friction and windage losses can be included in the calculation by using thermally expanded rotor geometry data in (3) and (4). Whereas thermal expansion of the bandage is negligible, expansion of metal rotor parts such as rotor iron and magnets will put a big strain on the bandage. Additional tangential stress due to rotation of the thin bandage with mass density ρ_b at overspeed $\omega_{\text{overspeed}}$, which can be treated as a rotating ring, is given by (5a). If the bandage is considered as a thick shell, the tangential stress depends on the radius. For the inner radius r_i, where the tangential stress is maximum, it is given by (5b). The additional centrifugal forces on magnets and bandage each reduce the total contact pressure between rotor and magnets by (6) and (7), with radius r, mass density ρ, and height h of magnet (m) and bandage (b), respectively, i.e.,

$$\sigma_{t,\omega} = \rho_b \cdot \omega_{\text{overspeed}}^2 \cdot r^2 \quad \text{(thin shell)} \quad (5a)$$

$$\sigma_{t,\omega}(r_i) = 0.4125 \cdot \rho_b \cdot \omega_{\text{overspeed}}^2 \cdot (0.424 r_i^2 + 2 r_a^2) \quad \text{(thick shell)} \quad (5b)$$

$$p_{\omega,m} = r_m \cdot \rho_m \cdot \omega_{\text{overspeed}}^2 \cdot h_m \quad (6)$$

$$p_{\omega,b} = r_b \cdot \rho_b \cdot \omega_{\text{overspeed}}^2 \cdot h_b. \quad (7)$$

TABLE II
ROTOR GEOMETRY FOR TWO DIFFERENT ROTOR CONFIGURATIONS

Rotor	M1	M2
rotor outer diameter d_a	88.6 mm	83.6 mm
pole coverage ratio α_e	**0.87**	**1.00**
air gap δ	0.7 mm	3.2 mm
thickness of bandage h_b	5.7 mm	4.8 mm
magnet height h_m	7.0 mm	4.5 mm
bandage undersize ΔD	0.24 mm	0.13 mm
mounting of bandage	axial pressing	cold shrinking at –190°C
bandage stress limit $\sigma_{t,max}$	1100 N/mm^2	1100 N/mm^2

III. EXAMPLE OF A HIGH-SPEED MOTOR WITH 40 kW AT 40 000 r/min

For a magnetically levitated PMSM with $P_N = 40$ kW, rated speed $n_N = 40\,000$ r/min, two different rotors with surface-mounted Sm_2Co_{17} magnets have been designed and built. The rotor circumferential speed at overspeed $n = 1.2 \cdot n_N = 48\,000$ r/min is $v_u = 222$ m/s. The main parameters of the two rotors are shown in Table II.

A. Design of Rotor M1

To limit the magnitude of air gap flux density harmonics, rotor M1 (Fig. 3) is built with a pole coverage ratio of $\alpha_e = 87\%$. To avoid eddy currents, the interpole gap of rotor M1 is filled with a nonconducting resin mass with a low mass density of 1.3 g/cm^3 compared with a mass density of the magnets of $\rho_m = 8.3$ g/cm^3. This causes a considerable variation of radial

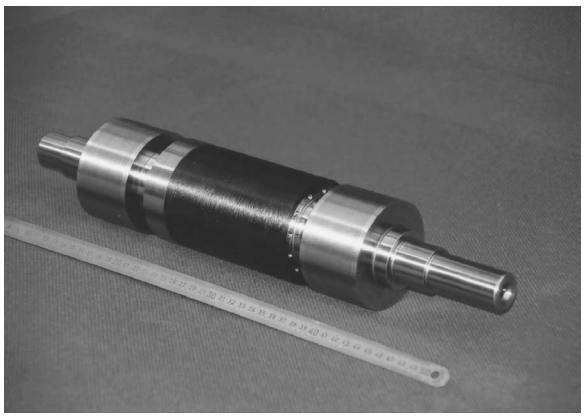

Fig. 3. Rotor M1, $n_N = 40\,000$ r/min, magnetic levitation, carbon-fiber bandage.

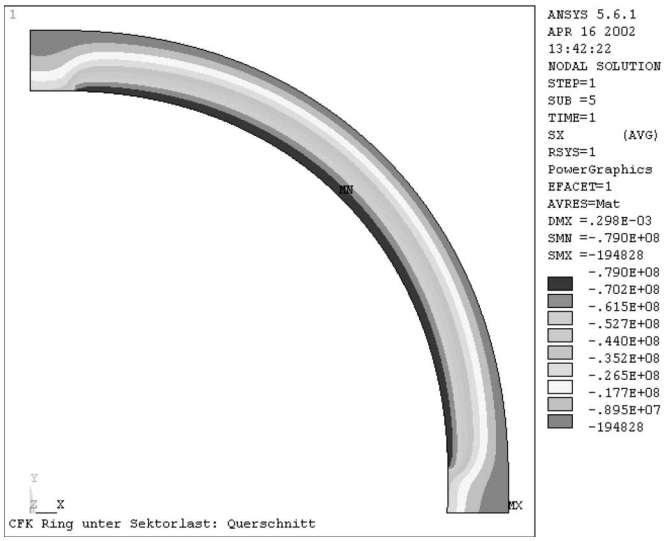

Fig. 4. Calculated radial stress variation σ_r inside the bandage of rotor M1 at $n = 40\,000$ r/min and $\vartheta = 150$ °C.

bandage stress along the circumference, leading to additional bending forces in the carbon fiber (Fig. 4). This bending stress is not included in (1)–(6), so that more sophisticated calculations, considering also orthotropic behavior of the fiber material and bending forces, or FE calculations are required (Fig. 5). In this case, (1)–(6) yield too low values for the tensile stress (Fig. 5, cases 1 and 2). Residual contact pressure at overspeed and $\vartheta_{\mathrm{rotor}} = 150$ °C is calculated as $p_c = 29.4$ N/mm^2. The analytical result for tangential bandage stress, treating the bandage as a thick shell, is $\sigma_t = 669.3$ N/mm^2. In addition, local stress due to the edges of the magnets, which are of rectangular cross section, must be added. Thus, the von Mises equivalent stress might be surpassing the indicated stress limit at overspeed 48 000 r/min. Note that prestress and thermal expansion are the dominating effects on bandage stress.

In Fig. 5, case 5, FE calculation results show that rotor M1 has a very small tangential stress safety margin at overspeed. In fact, rotor M1 crashed during a no-load test already at a rotational speed of 35 000 r/min. According to the previous calculations, M1 should have been able to withstand the mechanical stress at that speed. Investigations on the crashed

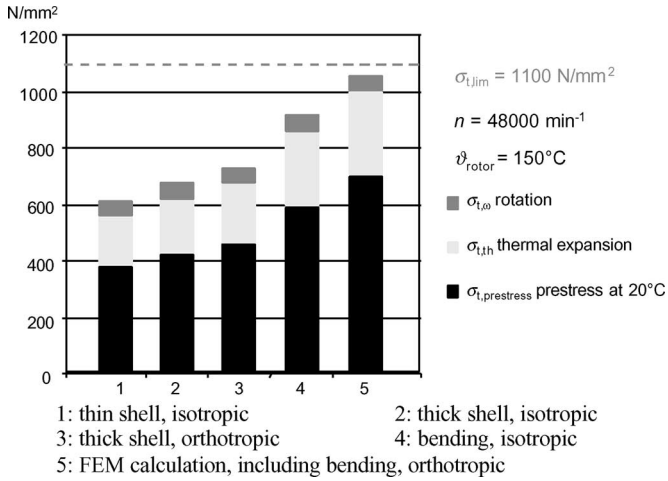

Fig. 5. Calculated tangential bandage stress σ_t for different bandage models.

Fig. 6. Rotor M1 after the bandage crash at $n = 35\,000$ r/min.

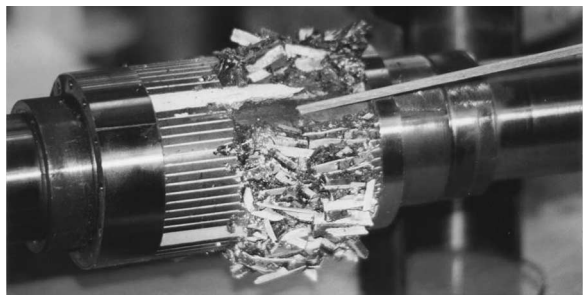

Fig. 7. Destruction of brittle magnets underneath the broken bandage.

rotor revealed that the bandage broke along the edge of one magnetic pole. Fig. 6 shows the destroyed bandage after the crash. The main destruction is visible in the form of a fracture along the edge of a pole gap along two-thirds of the active iron length, whereas the remaining part of the bandage shows only minor destruction at the surface due to friction, when touching the stator bore. A first assumption of improper bandage manufacturing including cavities inside the carbon-fiber resin matrix could be disproved by microscopic investigations. Thus, the bandage itself was in proper conditions. Removal of the bandage revealed that the brittle Sm_2Co_{17} magnets underneath the bandage were not able to withstand the massive impact during the bandage failure (Fig. 7). The magnets were axially arranged in three rows. Two rows of magnets were destroyed

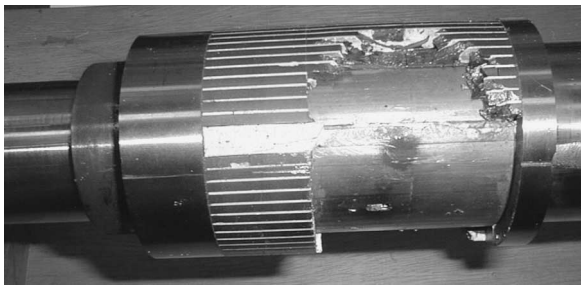

Fig. 8. Local heating spot underneath the magnets after bandage failure.

by the crash. In Fig. 7, two pole gaps filled with resin mass are also visible. The pointer shows the location of the bandage failure, which is adjacent to one of the pole gaps. A black spot underneath the magnets next to the pole gap in Fig. 8 indicates massive rotor heating at this point during the failure, showing that this is the point of maximum destruction. In Fig. 5, it is also visible that bandage stress is mainly caused by prestress due to stretching of the bandage and due to thermal expansion of the rotor at elevated temperature. In Fig. 5, a rotor temperature of 150 °C is assumed for the stress calculation, which increases the total stress acting on the bandage sleeve by 50% compared with prestress at 20 °C. The rotor temperature of motor M1 at the time of the rotor failure was not monitored, as it is difficult to measure the temperature of a magnetically suspended rotor without introducing slip rings. Therefore, it is possible that the rotor was heated up to temperatures above 150 °C. In the first test, the motor was operated at no load without a sine-wave filter for about 90 min, so that stator current harmonics might have heated up the massive rotor yoke, causing too high rotor temperatures. Furthermore, axial pressing of the bandage can be very harmful to the carbon-fiber material. In case of rotor M1, the carbon-fiber sleeve with an undersize of $\Delta D = 0.24$ mm has been axially pressed onto the rotor using a total force of 225.6 kN. This causes a shear stress and can destroy the inner layer of carbon fibers and lead to a weakening of the bandage in total.

In summary, we can state that a number of effects were involved in the rotor crash. The influences of bandage weakening due to axial pressing and rotor heating are difficult to evaluate as, e.g., the rotor temperature was not measured. However, the location of the bandage failure adjacent to the interpole gap as shown in Figs. 6–8 clearly indicates that the rotor crash was triggered by a local failure of the bandage at the edge of a pole gap. This corresponds to the location of maximum tangential stress obtained from FE calculations as shown in Fig. 4. Bending effects and the additional "edge effect" of the magnets, cutting into the carbon fiber along with the small safety margin shown in Fig. 5, can therefore be seen as the main causes for the rotor crash. The bending effect can be avoided by filling the pole gap with a material similar to the magnets instead of resin.

B. Design of Rotor M2

To improve the mechanical strength, the second rotor M2 experienced some major design changes compared with rotor M1 (Fig. 9; Table II). First, the interpole gap has been avoided

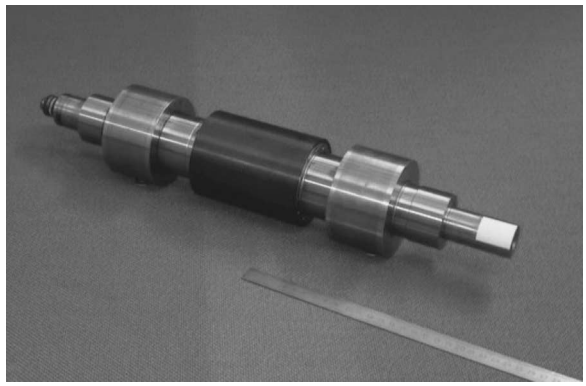

Fig. 9. Improved rotor M2, $n_N = 40\,000$ r/min, magnetic levitation.

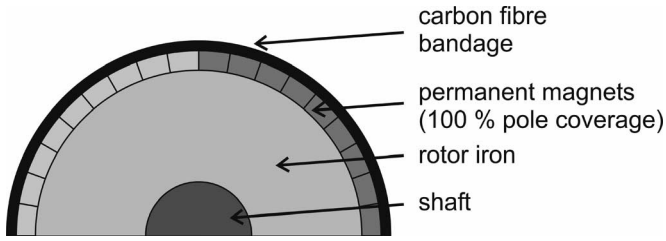

Fig. 10. Surface-mounted magnet PMSM without interpole gap (M2).

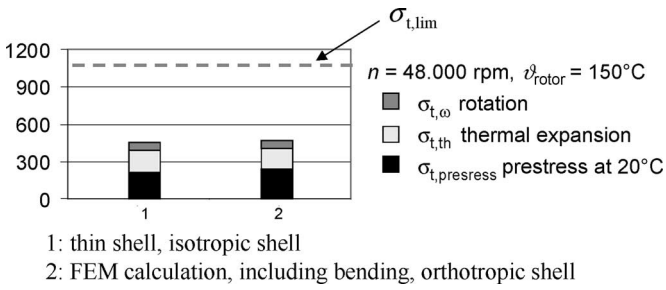

Fig. 11. Calculated tangential bandage stress σ_t of rotor M2.

$(\alpha_e = 100\%)$, as shown in Fig. 10. This means that the magnets are evenly distributed along the circumference, thus achieving rotational symmetry without any bending effect. In this case, (1)–(6) lead to satisfying results, which can be verified by an FE calculation (Fig. 11). Furthermore, the air gap has been increased from $\delta_{\mathrm{M1}} = 0.7$ mm to $\delta_{\mathrm{M2}} = 3.2$ mm to reduce the air friction losses inside the air gap and hence reduce rotor heating. The magnet height has been reduced from $h_{m,\mathrm{M1}} = 7$ mm to $h_{m,\mathrm{M2}} = 4.5$ mm, which still provides a sufficient demagnetization reserve but reduces the centrifugal forces acting on the magnets. Due to lower flux density, an increased current loading is necessary to keep the output power unchanged. Reducing the bandage sleeve undersize from $\Delta D_{\mathrm{M1}} = 0.24$ mm to $\Delta D_{\mathrm{M2}} = 0.13$ mm also allowed for a more gentle procedure to mount the bandage onto the rotor structure. The rotor has been cooled with liquid nitrogen LN_2 to a temperature of -190 °C. Due to rotor shrinking, the bandage could be mounted onto the rotor without any axial pressure. Rotor expansion during thermal adaptation to room temperature caused the stretching of the bandage and thus the generation of prestress. The carbon-fiber material is very strong in terms of tangential stress while being very sensitive to bending forces. As glass-fiber composite is less

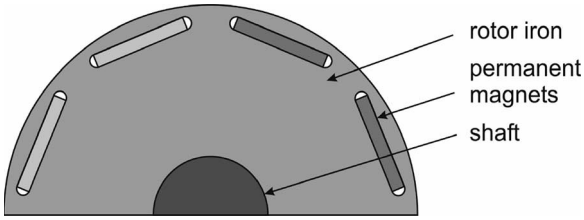

Fig. 12. PMSM with buried magnets.

sensitive to bending stress, a thin layer of glass-fiber bandage has been introduced to the inner layer of the bandage to withstand bending effects due to segmented magnets. Fig. 11 shows the results of the calculations using (1)–(7). The maximum tangential stress (thin shell) is only $\sigma_t = 491$ N/mm^2, thus giving a large safety margin to the bandage stress limit of $\sigma_{t,\max} = 1100$ N/mm^2 and is therefore fulfilling condition (2). The residual contact pressure at overspeed $n = 48\,000$ r/min and 150 °C is $p_c = 13.1$ N/mm$^2 > 0$, which is in accordance to condition (1). As no bending stress occurs in this design due to the rotational symmetry, these analytical results are met by FE calculations, which are also shown in Fig. 9. Noncontact rotor temperature monitoring was also implemented in rotor M2 and revealed rotor temperatures of 90 °C at rated load, i.e., 24 000 r/min, showing that rotor heating is below 150 °C. This rotor has been built and successfully tested up to rated speed of $n_N = 40\,000$ r/min. Detailed information about the performance of this motor is given in [4].

IV. Mechanical Design of Buried Magnet High-Speed Machines

If the permanent magnets are "buried" within the rotor iron, the rotor iron itself fixes the magnets (Fig. 12). No carbon- or glass-fiber bandage is needed, thus reducing the total air gap and the required amount of magnet material. Exact analytical calculation of the mechanical stress inside the iron sheet is difficult; therefore, FE calculations are recommended [5]. However, for simple magnet arrangements with buried magnets as shown in Fig. 10, analytical approaches using an equivalent ring arrangement can still give a good estimate about the mechanical stress. The magnets are inserted into the slots, so no prestress is given. The outer iron bridge must withstand its own centrifugal forces and that of the magnets. Thermal expansion of iron and magnets is similar, so the temperature influence on stress is small. An analytical approach to calculate the mechanical stress on the rotor structure is shown in Fig. 13. The centrifugal forces acting on the magnets and the covering iron bridge are transferred to an equivalent ring with an artificially increased mass density ρ_{equiv} [6]. The height of the equivalent ring section h_{equiv} is chosen to be equal to the narrowest height of the iron bridge that covers the magnets. First, the increased mass density of the equivalent ring is determined as

$$\rho_{\text{equiv}} = \rho_{\text{Fe}} \cdot \frac{A_{\text{magnet}} + A_{\text{Fe},o}}{A_{\text{equiv}}}. \tag{8}$$

Both the masses of the magnet and the iron that covers the magnet are transformed into the equivalent ring. Thereby, it is assured that the equivalent ring suffers from the same

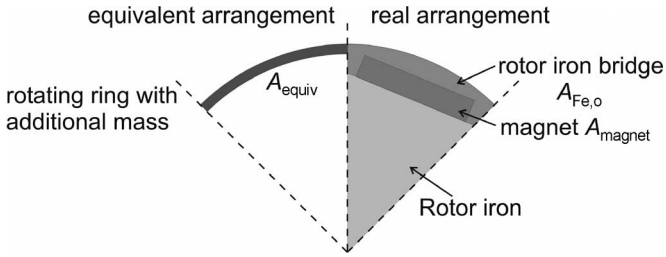

Fig. 13. Equivalent ring section with increased mass density representing the rotating magnet and the iron bridge.

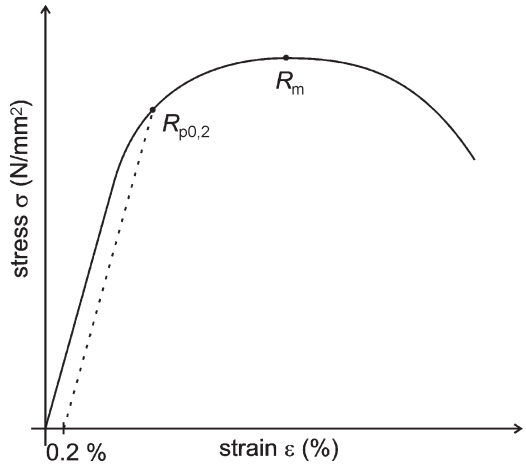

Fig. 14. Typical stress–strain characteristic $\sigma(\varepsilon)$ of iron material.

centrifugal forces as the original arrangement. With the outer and inner radii of the equivalent ring, i.e., $r_{\text{equiv},o}$ and $r_{\text{equiv},i}$, respectively, the tangential stress inside the equivalent ring under rotation at overspeed can be determined as

$$\sigma_{t,\text{equiv}} = \left(\frac{r_{\text{equiv},o} + r_{\text{equiv},i}}{2}\right)^2 \cdot \omega^2_{\text{overspeed}} \cdot \rho_{\text{equiv}}. \tag{9}$$

So far, the calculation does not pay attention to local peak stress caused by the uneven distribution of the magnets and the shape of the magnet edges. By designing round-shaped slot edges, the increase of stress at these edges caused by the notch effect can be limited to about 100% (factor 2). Therefore, the maximum mechanical stress is located at the slot edges, i.e.,

$$\sigma_{t,\max} = 2 \cdot \sigma_{t,\text{equiv}}. \tag{10}$$

The stress–strain characteristic $\sigma(\varepsilon)$ of iron is nonlinear as shown in Fig. 14. The maximum tensile stress inside the iron must stay below the iron sheet yield strength $R_{p0.2}$. A typical value for $R_{p0.2}$, e.g., for M270-35A sheets, is $R_{p0.2} = 450$ N/mm^2. This means that putting a stress of $R_{p0.2}$ to the material will lead to a permanent (irreversible) relative deformation of 0.2%. This is accepted as permanent deformation of the iron sheets and therefore defines the limit of the stress that can be applied to the material. With special high-strength materials, yield strength can reach values of up to $R_{p0.2} = 850$ N/mm^2 [7].

Thus, the maximum permissible stress inside the rotor iron is

$$\sigma_{t,\max} = 2 \cdot \sigma_{\text{equiv}} < R_{p0.2}. \tag{11}$$

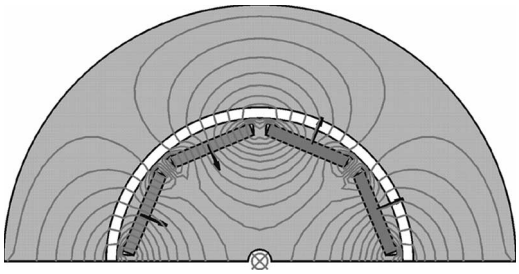

Fig. 15. Equivalent rotor design to M2 using buried magnets. No-load field plot with neglected stator slotting.

TABLE III
ROTOR GEOMETRY FOR BURIED MAGNET ROTOR DESIGN, M3

Rotor	M3
rotor outer diameter d_a	83.6 mm
air gap δ	3.2 mm
magnet height h_m	3.6 mm
magnet width b_m	25 mm
minimum height of iron bridge	1.66 mm
iron yield strength	450 N/mm^2

A. Example for the Calculation of the Mechanical Strength of a Buried Magnet Rotor

To compare the mechanical behavior of surface-mounted and buried magnet PMSM, an alternative design to the previously discussed surface-mounted magnet PMSM (rotor M2) is considered (Fig. 15). To obtain a comparable design M3, the rotor diameter, the mechanical air gap, and the fundamental of the air gap flux density are kept unchanged. The nonlinear magnetic circuit including iron saturation has been designed using FE calculations. The dimensions of design M3 are listed in Table III. The thickness of the iron bridge at the narrowest location is 1.66 mm.

According to the previous explanations, this is also the value chosen for the height of the equivalent ring h_{equiv}. With the dimensions given in Table III, the cross-sectional area of one magnet and its covering iron amounts to

$$A_{\mathrm{magnet}} + A_{\mathrm{Fe},o} = 184.5\ \mathrm{mm}^2 \tag{12}$$

whereas the cross-sectional area of the equivalent ring section is

$$A_{\mathrm{equiv}} = \pi(r^2_{\mathrm{equiv},o} - r^2_{\mathrm{equiv},i})/8 = 53.4\ \mathrm{mm}^2. \tag{13}$$

Hence, the mass density of the equivalent ring section is

$$\rho_{\mathrm{equiv}} = \frac{A_{\mathrm{magnet}} + A_{\mathrm{Fe},o}}{A_{\mathrm{equiv}}}\rho_{\mathrm{Fe}} = 3.45 \cdot \rho_{\mathrm{Fe}} = 26.9 \times 10^3\ \frac{\mathrm{kg}}{\mathrm{m}^3}. \tag{14}$$

Finally, we get a tangential stress inside the equivalent ring due to rotation at overspeed $n = 48\,000$ r/min of

$$\sigma_{t,\mathrm{equiv}} = 1141\ \frac{\mathrm{N}}{\mathrm{mm}^2}. \tag{15}$$

Including the effect of the slot shape (10), the total tangential stress inside the rotor iron at the magnet edges will be $\sigma_{t,\max} = 2282$ N/mm^2, which is far higher than the typical yield strength

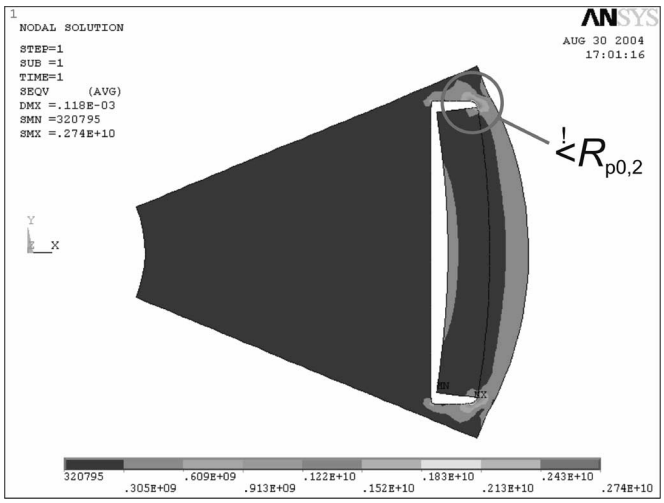

Fig. 16. FE result for von Mises stress at $n = 48\,000$ r/min.

of the iron sheet material $R_{p0.2} = 450$ N/mm^2 (M270-35A). Even with high strength material, this value would still exceed the yield strength limit. FE calculation (Fig. 16) resulted in maximum values for von Mises stress of 2700 N/mm^2. This value strongly depends on the exact shape of the slot edges. In Fig. 16, the outer slot edges are shaped with a small radius of only 0.5 mm. The maximum stress at the slot edge can be influenced by using a bigger radius at the slot edges (e.g., $h_m/2$).

As the value of the tangential stress clearly exceeds the yield strength limit $R_{p0.2}$ of typical electrical steel sheets, (8)–(10) can also be used to determine the maximum permissible speed of rotor M3, i.e.,

$$n_{\mathrm{overspeed,max}} = \sqrt{\frac{\sigma_{t,\mathrm{equiv,max}}}{r^2 \cdot \rho_{\mathrm{equiv}} \cdot 4\pi^2}}. \tag{16}$$

Using M270-35A sheets and considering the stress increase at the magnet edges, $\sigma_{t,\mathrm{equiv,max}}$ will be $R_{p0.2}/2 = 225$ N/mm^2. Thus, for maximum permissible overspeed, we get $n_{\mathrm{overspeed}} = 21\,317$ r/min, finally giving a maximum rated speed of $n_N = 17\,764$ r/min, which is far less than the maximum speed of a surface-mounted magnet rotor with a carbon-fiber bandage.

V. CONCLUSION

During the design procedure of high-speed electrical machines, special attention needs to be paid to mechanical design issues. Although, in many cases, FE calculations for the mechanical strength of the rotor structure are recommended, for simple but realistic rotor structures, analytical approaches lead to satisfying results. This holds true both for surface-mounted and specially selected buried-magnet-type rotors. The fixation of magnets in surface-mounted and buried magnet-type high-speed permanent-magnet machines is compared for the same motor data, showing that for high-speed operation (e.g., 40 000 r/min, 40 kW), surface-mounted magnets fixed by a carbon-fiber bandage are the better choice, as they incorporate much higher mechanical strength, allowing higher maximum speed.

REFERENCES

[1] *Product Properties,* Tenax Fibres, Wuppertal, Germany, 1998.

[2] M. Klohr and A. Binder, "Design of carbon fiber bandages for high speed permanent magnet rotors," in *Proc. SPEEDAM*, Ravello, Italy, Jun. 11–14, 2002, pp. B7/13–B7/18.

[3] W. Beitz and K.-H. Grote, *Dubbel–Taschenbuch für den Maschinenbau*, 19th ed. Berlin, Germany: Springer-Verlag, 1997.

[4] A. Binder, M. Klohr, and T. Schneider, "Losses in high speed permanent magnet motor with magnetic levitation for 40 000/min, 40 kW," in *Proc. 16th ICEM*, Krakow, Poland, Sep. 5–8, 2004, vol. 1, pp. 93–94.

[5] E. Lovelace, T. Jahns, T. Keim, and J. Lang, "Mechanical design considerations for conventionally laminated, high-speed, interior PM synchronous machine rotors," *IEEE Trans. Ind. Appl.*, vol. 40, no. 3, pp. 806–812, May/Jun. 2004.

[6] C. Schätzer, "Ein Verfahren zur Optimierung bei elektrischen Maschinen mit Hilfe der numerischen Feldberechnung," Ph.D. dissertation, Dept. Elect. Eng. Inf. Technol., Inst. Elect. Energy Conversion, Darmstadt, Germany, 2001.

[7] Y. Honda, S. Yokote, T. Higaki, and Y. Takeda, "Using the halbach magnet array to develop an ultrahigh-speed spindle motor for machine tools," in *Proc. IEEE IAS Annu. Meeting*, New Orleans, LA, Oct. 5–9, 1997, pp. 56–60.

Andreas Binder (M'97–SM'04) received the Dipl.-Ing. (diploma) and Dr.Techn. (Ph.D.) degrees in electrical engineering from the University of Technology, Vienna, Austria, in 1981 and 1988, respectively.

From 1981 to 1983, he was with ELIN-Union AG, Vienna, working on synchronous generators design. From 1983 to 1989, he was a Researcher with the Department of Electrical Machines and Drives, Technical University, Vienna. From 1989 to 1997, he led a group developing dc and inverter-fed ac motors and drives at Siemens AG, Bad Neustadt and Erlangen, Germany. Since 1994, he has been a Lecturer with the University of Technology, Vienna (*venia docendi*). Since October 1997, he has been the Head and a Full Professor with the Institute of Electrical Energy Conversion, Darmstadt University of Technology, Darmstadt, Germany, where he is responsible for teaching and research for electrical machines, drives, and railway systems. Since 1999, he has been the Head of the Electrical Machines, Drives, Mechatronics section of the German Association of Electrical Engineers (VDE). He is the author or coauthor of 120 scientific publications. He is the holder of several patents.

Dr. Binder received the Energietechnische Gesellschaft im VDE (ETG)-Literature Award of the VDE in 1997. He is a member of the VDE, Institution of Electrical Engineers, U.K., Verband Deutsche Ingenieure (VDI), and European Power Electronics and Drives Association (EPE).

Tobias Schneider received the Dipl.-Ing. degree from Darmstadt University of Technology, Darmstadt, Germany, in 2002. He is currently working toward the Ph.D. degree in electrical engineering at the Institute of Electrical Energy Conversion, Darmstadt University of Technology, where he is involved in research on bearingless motors in high-speed applications.

Markus Klohr received the Dipl.-Ing. degree from Darmstadt University of Technology, Darmstadt, Germany, in 1998. He is currently working toward the Ph.D. degree in electrical engineering at the Institute of Electrical Energy Conversion, Darmstadt University of Technology, where he was involved in research on high-speed machines with magnetic bearings.

He is currently with Bombardier Transportation, Mannheim, Germany.